An Integrated System for the Segmentation of Atherosclerotic Carotid Plaque Ultrasound Video

Christos P. Loizou, *Senior Member, IEEE*, Styliani Petroudi, *Member, IEEE*, Marios Pantziaris, Andrew N. Nicolaides, and Constantinos S. Pattichis, *Senior Member, IEEE*

Abstract—The robust border identification of atherosclerotic carotid plaque, the corresponding degree of stenosis of the common carotid artery (CCA), and also the characteristics of the arterial wall, including plaque size, composition, and elasticity, have significant clinical relevance for the assessment of future cardiovascular events. To facilitate the follow-up and analysis of the carotid stenosis in serial clinical investigations, we propose and evaluate an integrated system for the segmentation of atherosclerotic carotid plaque in ultrasound videos of the CCA based on video frame normalization, speckle reduction filtering, M-mode state-based identification, parametric active contours, and snake segmentation. Initially, the cardiac cycle in each video is identified and the video M–mode is generated, thus identifying systolic and diastolic states. The video is then segmented for a time period of at least one full cardiac cycle. The algorithm is initialized in the first video frame of the cardiac cycle, with human assistance if needed, and the moving atherosclerotic plaque borders are tracked and segmented in the subsequent frames. Two different initialization methods are investigated in which initial contours are estimated every 20 video frames. In the first initialization method, the initial snake contour is estimated using morphology operators; in the second initialization method, the Chan–Vese active contour model is used. The performance of the algorithm is evaluated on 43 real CCA digitized videos from B-mode longitudinal ultrasound segments and is compared with the manual segmentations of an expert, available every 20 frames in a time span of 3 to 5 s, covering, in general, 2 cardiac cycles. The segmentation results were very satisfactory, according to the expert objective evaluation, for the two different methods investigated, with true-negative fractions (TNF-specificity) of $83.7 \pm 7.6\%$ and $84.3 \pm 7.5\%$; true-positive fractions (TPF-sensitivity) of $85.42 \pm 8.1\%$ and $86.1 \pm 8.0\%$; and between the ground truth and the proposed segmentation method, kappa indices (KI) of 84.6% and 85.3% and overlap indices of 74.7% and 75.4%. The segmentation contours were also used to compute the cardiac state identification and radial, longitudinal, and shear strain indices for the CCA wall and plaque between the asymptomatic and symptomatic groups were investigated. The results of this study show that the integrated system investigated in this study can be successfully used for the automated video segmentation of the CCA plaque in ultrasound videos.

I. Introduction

THE size and composition of carotid atherosclerotic plaque have been shown to be independent predictors of future cardiovascular events [1], with vulnerable plaques described as containing a large lipid core, a thin fibrous cap, and dense macrophage inflammation in or beneath its surface, whereas stable plaques are characterized by larger quantities of calcium and collagen and less lipids and inflammatory cells [2]. Accurate and precise segmentation of the atherosclerotic carotid plaque in ultrasound B-mode video [see Fig. 1(a)] allows for the extraction of different anatomical properties of the artery wall, and plaque that can be most useful to the physicians for the evaluation of plaque development and the process of atherosclerosis in modeling and evaluating the risks for future cardiovascular events. Ultrasound, elastography, and other imaging methods such as spectroscopic photoacoustic imaging can be integrated to advance the characterization of the plaques and corresponding vulnerability [3] because the variation in the mechanical properties of the different tissue types is huge [4]. For example, the elasticity modulus of calcified plaque material is 50 times higher than the modulus of cellular plaque tissue [1]. Over the past few years, different quantitative methods have been developed for the common carotid artery (CCA) segmentation [5], [6], as well as plaque heterogeneity and plaque echogenicity characterization [2]– [5].

The availability and evaluation of different characteristics of carotid plaque is of outmost importance especially because it is widely accepted that the experts are only moderately confident that there is adequate evidence to determine which interventions to use for different patient populations [3]. However the manual segmentation of the plaque in the CCA in ultrasound video [see also Fig. 1(h)], or over large sequences of images is not only a tedious and time consuming task, but also suffers from large inter- and intra-observer variability and it is difficult to trace boundaries for each time frame of the cardiac cycle and for large volume of data sets [6], [7]. Polak *et al.* [8] demonstrated that when expert operators manually delineate the intima and adventitia borders of the CCA, errors can be considerable and are different for the intima and the adventitia borders. The errors are further amplified when experts manually delineate atherosclerotic carotid plaques. Thus, the need exists for the development of new automated or
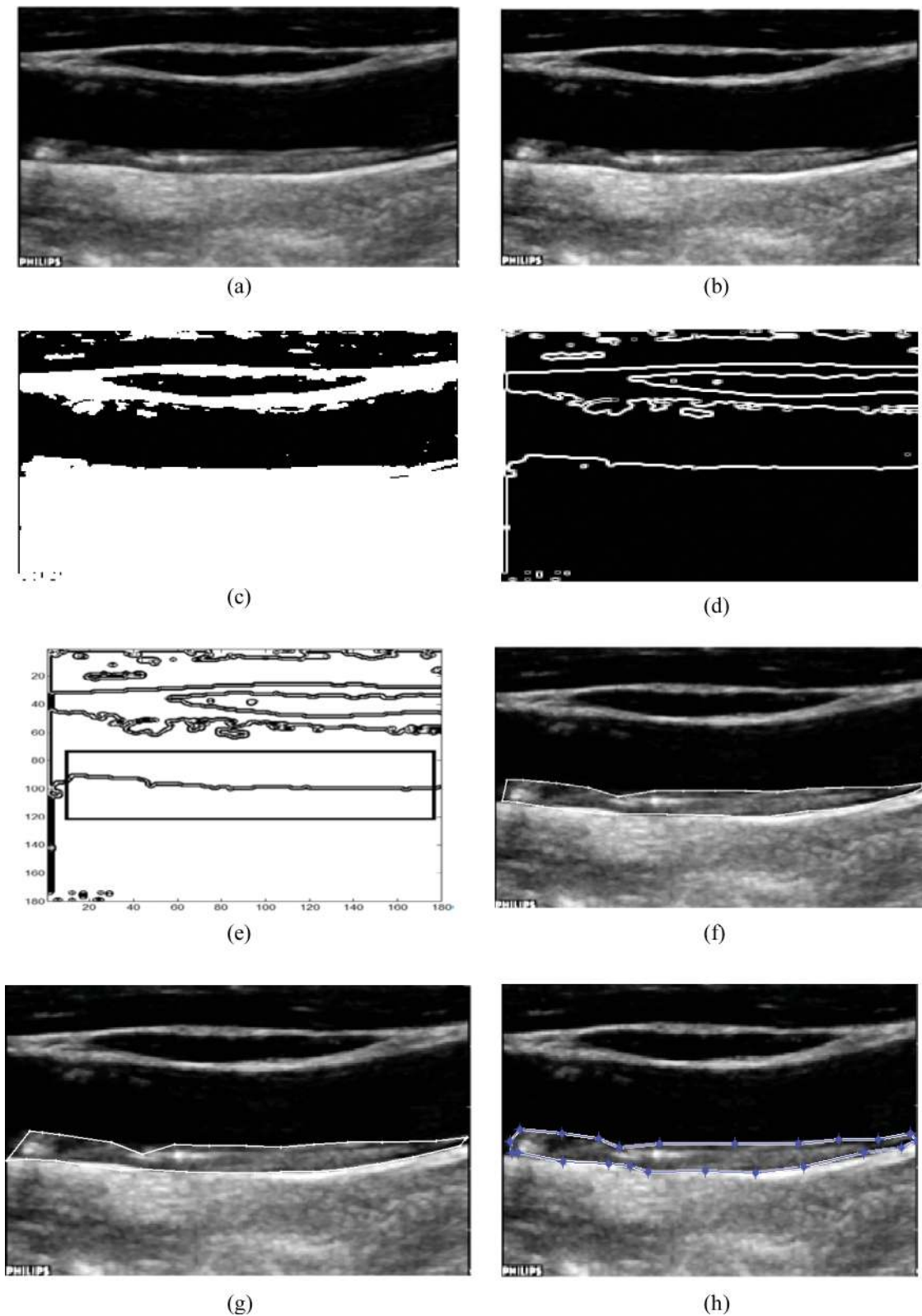
(a)

(b)

(c)

(d)

(e)

(f)

(g)

(h)

Fig. 1. Plaque contour initialization procedure and final snake contour: (a) First frame of the original ultrasound CCA video, (b) normalized despeckled frame image with the DsFlsmv filter (2 iterations, window 3×3), (c) binary image frame after dilation with a square window shape of size 9×9 after removing edges, (d) edge image frame after removal of erroneous edges, (e) ROI manual positioning and interpolating spline and detected initial contour with contour selection, (f) initial snake contour mapped on the first video frame, (g) final snake contour after snake deformation, and (h) manual delineation of plaque.

TABLE I. An Overview of Atherosclerotic Carotid Plaque Segmentation Techniques.

Study	Segmentation Method	AIC	N
Ultrasound imaging 2-D			
Hamou [14]	Canny edge detection	No	—
Abdel-Dayen [15]	Morphological based	No	—
Mao [16]	Discrete dynamic contour	No	7
Abolmaesumi [17]	Kalman filtering	No	1
Gill [19]	Balloon	No	2
Loizou [6]	Active contour model	Yes	80
Delsanto [21]	Gradient based snake with fuzzy k-means	Yes	56
Golemati [22]	Hough transform	No	4
Ultrasound video			
Destrempes [7]	Bayesian model	No	33
Ultrasound imaging 3-D			
Zahalka [23]	Geometrically deformable model	Yes	1
Ukwatta [24]	Level sets	No	21

AIC = automatic initial contour; N = number of cases investigated.

semi-automated tools and techniques for the assessment of the risk of stroke from ultrasound videos of the CCA incorporating plaque segmentation.

The predictive ability to identify which patients will have a stroke is poor, where the current practice of assessing the risk of stroke relies on measuring the thickness of the CCA wall [intima-media-thickness (IMT)] [9], [10] or the artery lumen stenosis by identifying the plaque borders in the carotid artery [6]. Although the IMT and the degree of stenosis can reliably be delineated in still B-mode ultrasound images [1], [6], [9], [10], the moving borders of the atherosclerotic carotid plaque and the identification of the systolic and diastolic video states [7] may provide additional information of an individual's stroke risk, and treatment of asymptomatic patients may be improved [11].

We propose in this study an integrated system for the video segmentation of the CCA based on our previous work [6], [10], to further facilitate the quantitative assessment of atherosclerosis disease. The main extension to our previous work in [6], which was based on still image segmentation, is the consideration of moving frames, the identification of the states diagram of the video, the extraction of systolic and diastolic states [7], and the automated re-initialization of the snake contour every 20 frames based on recent work presented in [10]. Preliminary results of this study were also published in [12], where we proposed an improved initialization method for the positioning of the initial snake contour. The snake contour was repositioned using the level-set formulation of Chan and Vese [13], using random initialization, which provided a segmentation of the CCA ultrasound image sequences into different distinct regions, one of which corresponds to the carotid wall region above the lumen, and another which corresponds to the carotid wall region below the lumen, including the plaque borders. The key point of the proposed framework is the accuracy of the initialization.

To the best of the authors' knowledge there is only one published study for the segmentation of atherosclerotic carotid plaque in ultrasound CCA videos [7]. The method by

Destrempes et al. [7] is based on a Bayesian segmentation model and is evaluated on 33 video sequences. Still, several other studies investigated the segmentation of atherosclerotic carotid plaque in ultrasound images. An overview of these techniques is given in Table I. Hamou and El-Sakka [14] proposed a method based on the Canny edge detector to detect the plaque in longitudinal CCA ultrasound images. A morphological-based approach for the carotid contour extraction was proposed in [15] for longitudinal ultrasound images of the CCA, incorporating speckle reduction filtering, contour quantization, morphological contour detection, and a contour enhancement stage. Mao et al. [16] proposed a discrete dynamic contour model for extracting the carotid artery lumen in 2-D transversal ultrasound images, whereas Abolmaesumi et al. [17] introduced a method, based on the star algorithm improved by Kalman filtering, for plaque segmentation in transversal carotid ultrasound images. A semi-automatic method for plaque segmentation in 3-D images of the CCA using the balloon model introduced in [18] was proposed by Gill et al. [19]. Loizou et al. [6] proposed a plaque segmentation method, based on the Williams and Shah snake [20], for the extraction of the CCA using an automated contour estimation and applied on 80 ultrasound images of the CCA. The atherosclerotic carotid plaque in [21], was segmented in 56 2-D longitudinal ultrasound images using a gradient-based snake segmentation method and fuzzy K-means algorithm with an initialization based on pixel intensity. In [22], the Hough transform was applied to perform segmentation of plaque in four 2-D cross-sectional ultrasound images of the CCA. In [23], an automated segmentation method for 3-D ultrasound carotid plaque based on a geometrically deformable model, taking advantage of both the local and regional detectors, was proposed. More recently, in [24], a 3-D semi-automated segmentation method using sparse field level sets, where the users choose anchor points on each boundary, was proposed for the segmentation of 3-D CCA images. All of these methods, with the exception of [7] (in which ultrasound video segmentation of the plaque in the CCA was proposed), have investigated and

proposed different solutions for the segmentation of the atherosclerotic carotid plaque in ultrasound images of the CCA.

As shown in Table I, different methods were investigated for the segmentation of the atherosclerotic carotid plaque in ultrasound images, yet these studies were evaluated on a limited number of subjects. Therefore, the need still exists for the development, implementation, and evaluation of an integrated system enabling the automated segmentation of ultrasound imaging carotid plaque.

In this paper, an integrated system for the segmentation of the atherosclerotic carotid plaque in 2-D ultrasound video of the common carotid artery (CCA) is presented and evaluated. The system builds on some of the authors' previous work [6], and incorporates image frame normalization, speckle reduction filtering, initial contour estimation, M-mode generation, and snake segmentation for the advancement of evaluation and treatment of the carotid atherosclerosis.

II. Materials and Methods

A. Recording of Ultrasound Videos

A total of 43 B-mode longitudinal ultrasound videos (from 38 asymptomatic subjects, aged 56 ± 12, and 5 symptomatic subjects, aged 53 ± 16; there were 17 female and 26 male subjects) of the CCA bifurcation of subjects were recorded representing different types of atherosclerotic plaque formation with irregular geometry typically found in this blood vessel. Almost all subjects demonstrated a left or a right CCA stenosis of 30% or larger. The videos were acquired by the ATL HDI-5000 ultrasound scanner (Advanced Technology Laboratories, Seattle, WA) and were recorded digitally on a magneto optical drive, with a size of 576×768 pixels with 256 gray levels, a pixel size of 59 μm (17 pixels/mm) and having a frame rate of 100 frames per second. This frame rate is high; however, it was used because these videos will also be analyzed for plaque motion estimation. The ATL HDI-5000 ultrasound scanner is equipped with a 256-element fine-pitch high-resolution 50-mm linear array and a multi-element ultrasound scan head with an extended operating frequency range of 5 to 12 MHz, and it offers real spatial compound imaging. The video segmentations were performed for 3 to 5 s intervals, covering, in general, 2 to 3 cardiac cycles.

B. Manual Plaque Segmentation

An expert neurologist with more than 20 years of clinical experience (coauthor Dr. M. Pantziaris) manually delineated the plaque borders between plaque and artery wall, and the borders between plaque and blood, every 20 frames on 43 longitudinal B-mode ultrasound videos of the CCA, after image normalization and speckle reduction fil-

tering (see Sections II-C and II-D), using Matlab software developed by our group [see Fig. 1(h)]. The manual segmentations traced in the first frame could be transferred to the second frame and then could be readjusted by the expert accordingly. In total, 538 (10 750 frames/20 = 538) ultrasound frames of the CCA were delineated. On average, 13 frames per video were manually delineated by the expert. The procedure used for carrying out the manual delineation was the one established and documented in the asymptomatic carotid stenosis and risk of stroke (AC-SRS) project protocol [25] for still images of the CCA. The correctness of the work carried out by a single expert was monitored and verified by at least one other expert. In cases in which several plaques were located in the CCA, comprising multiple components, each plaque was segmented independently so that each contour initialization represents a different plaque.

C. Video Normalization of Ultrasound Videos

Brightness adjustments of ultrasound videos were carried out based on the method introduced in [26]. This improves image compatibility by reducing the variability introduced by different gain settings, different operators, different equipment, and facilitates ultrasound tissue comparability [26]. Algebraic (linear) scaling of the first video frame was manually performed by linearly adjusting the image so that the median gray level value of the blood was 0 to 5 and the median gray level of the adventitia (artery wall) was 180 to 190 [26]. The intensity of the gray level values on the video frames ranged from 0 to 255. Thus, the brightness of all pixels in the video frame was readjusted according to the linear scale defined by selecting the two reference regions [see also Fig. 1(b)]. The subsequent frames of the video were then normalized based on the selection of the first frame. It is noted that a key point to maintaining a high reproducibility was to ensure that the ultrasound beam was at right angles to the adventitia, adventitia was visible adjacent to the plaque and that for image normalization, a standard sample consisting of half of the width of the brightest area of adventitia was obtained.

D. Speckle Reduction Filtering (DsFlsmv)

For speckle reduction, the filter DsFlsmv, introduced in [27], was applied to each consecutive frame prior to the plaque segmentation. The filters of this type utilize first-order statistics such as the variance and the mean of a pixel neighborhood and may be described with a multiplicative noise model [27], [28]. The moving window size for the despeckle filter DsFlsmv was 5×5 and the number of iterations applied to each video frame was two; a complete description of the filter and its parameters can be found in [27]–[30]. An example of the application of the DsFlsmv filter is shown in Fig. 1(b) after image normalization.
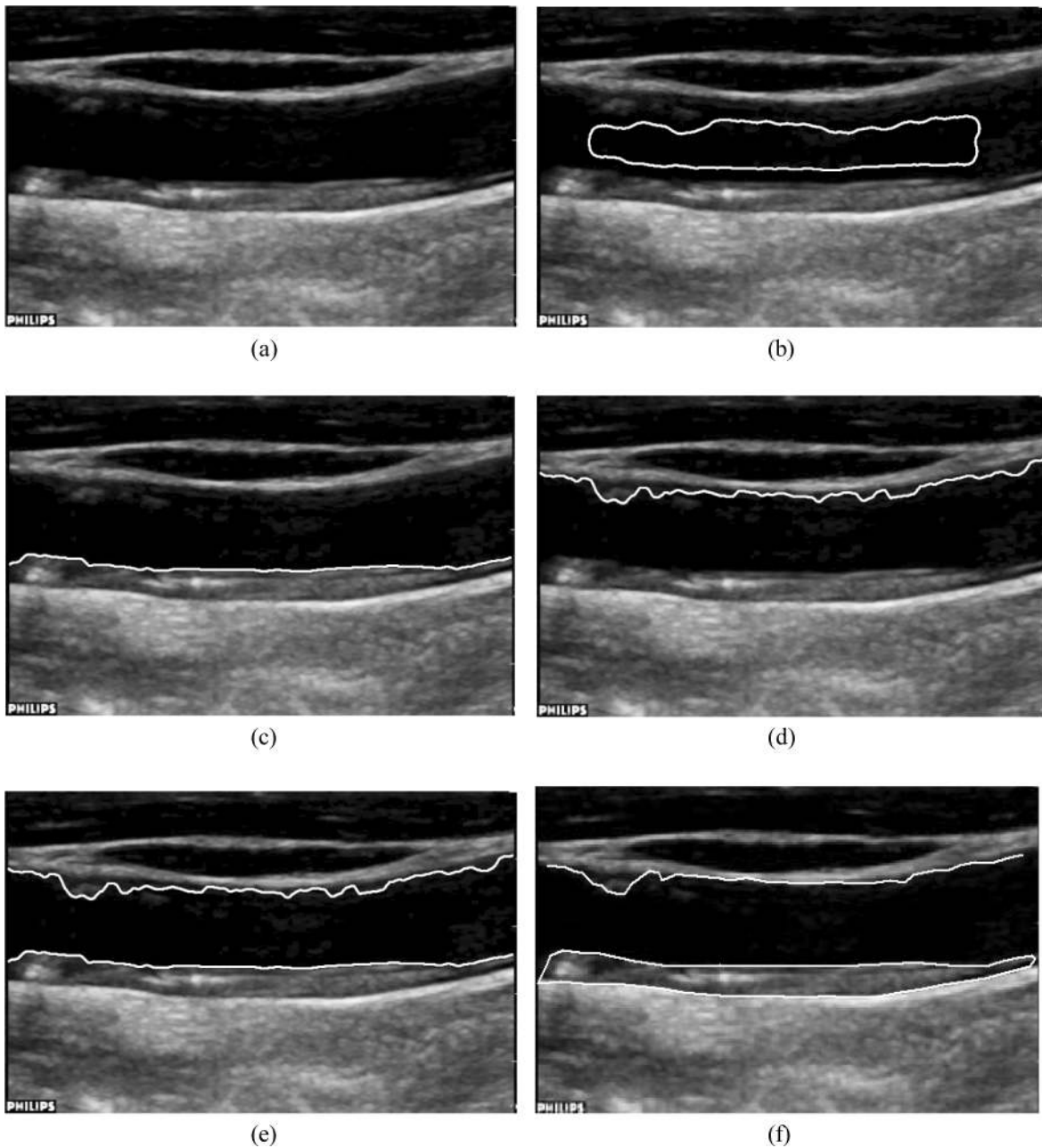
Fig. 2. (a) Original first frame of the video after normalization and despeckle filtering, (b) the Chan–Vese model initialization contour using simple thresholding and morphological closing, (c) and (d) the Chan–Vese model segmentation showing only initialization at the far and near wall of the CCA, respectively, (e) result of the Chan–Vese model (some morphological processing has been applied to the Chan–Vese result), and (f) final snake segmentation of plaque and lumen of the CCA.

E. Plaque Contour Initialization

Before running the video plaque snake segmentation algorithm, two different plaque initialization procedures (see also Figs. 1 and 2) were investigated for positioning the initial snake contour in the first frame of the video, as close to the area of interest (plaque borders) as possible. The two different initialization methods are explained in detail in the Appendix. Prior to both initialization methods, all the video frames were normalized (see Section II-B) and despeckled (see Section II-C). The normalized despeckled first video frame of a CCA video is shown in

Fig. 1(b). It is also assumed that the carotid artery is properly imaged in the video according to the standard clinical guidelines.

F. Snake Segmentation

The Williams and Shah snake segmentation method [20] was used to deform the snake and segment the plaque borders in each video frame. The snake contour, $v(s)$, adapts itself by a dynamic process that minimizes an energy function $[E_{\mathrm{snake}}(v,s)]$ defined as [20]

$$E_{snake}(v(s)) = E_{int}(\nu(s)) + E_{image}(v(s)) + E_{external}(v(s))$$
$$= \int_s (\alpha_s E_{cont}(v(s)) + \beta_s E_{curv}(v(s)) + \gamma_s E_{image}(v(s)) \quad (1)$$
$$+ E_{external}(v(s)))\mathrm{d}s.$$

where $E_{int}(v(s))$, $E_{image}(v(s))$, $E_{external}(v(s))$, $E_{cont}(v(s))$, and $E_{curv}(v(s))$ are the internal, image, external, continuity, and curvature energies of the snake, and α_s, β_s, and γ_s are the strength, tension, and stiffness parameters, respectively. The method was proposed and evaluated in [6] on 80 ultrasound images of the CCA and more details about the model can be found there. For the Williams and Shah snake, the strength, tension, and stiffness parameters were equal to $\alpha_s = 0.6$, $\beta_s = 0.4$, and $\gamma_s = 2$, respectively. This procedure was applied in cases where there was only one plaque present in the CCA video. In cases in which multiple plaques were located at the near or far wall of the CCA (22 out of 43 videos), thus forming multiple connected regions (see Fig. 3, left column), the proposed segmentation method was applied independently on each plaque component. The sampled contour points resulting from the previous step are used for the active contour initialization. The first and last points on the contour resulting from the initialization procedure presented in the previous section are connected to form a closed initial snake contour [see Figs. 1(g) and 2(f)]. The final plaque contour resulting from the snake deformation is mapped from the first video frame to the second and is sampled to provide the initialization for the snake deformation. The segmentation is carried out for a full cardiac cycle, which is identified using the procedure in Section II-G. Every 20 video frames, the entire initialization procedure is repeated to detect the plaque borders again, reposition the snake and reassure that the snake contour will not converge away from the area of interest. If there were multiple plaques in the CCA video, then the entire methodology is repeated for each plaque. Two more examples of video plaque segmentation are shown in Fig. 3.

G. M-Mode Image Generation, Boundary Extraction, State Identification, and Manual Delineation

The M-mode image [see Fig. 4(d)] can be generated in such a way that it crosses all plaque borders having maximum motion in opposite directions [31]. The procedure of the M-mode generation is illustrated in Fig. 4 and also described in [32].

Fig. 4(a) presents the first video frame of the cardiac cycle from a B-mode ultrasound video of the left CCA, after normalization and despeckle filtering acquired from a male symptomatic subject at the age of 64 (having a stent on the right CCA and a stenosis of 40% to 50%). Fig. 4(b) presents the automated snake segmentations of the plaque boundaries at the far wall of the CCA and the lumen segmentation at the near wall. The segmented atherosclerotic

plaque is shown in Fig. 4(c), whereas Fig. 4(d) presents the despeckled M-mode image generated from the CCA video for the first 1200 frames (12 s).

Perpendicular lines that cross the major axis of the plaque [from Fig. 4(c)], were placed automatically at the major axis quintiles (20%, 40%, 60%, and 80%). By scanning the intensity values along the straight perpendicular line selected by the user, the M-mode image is generated, by taking this line as the y-axis, and each frame of the video as the x-axis [see Fig. 4(d)]. Four M-mode images were generated for each of the corresponding four perpendicular lines. The manual delineations and all other measurements were performed (by M. Pantziaris) using a system implemented in Matlab from our group. The M-mode images were converted to binary images and morphological operators were applied to smooth the edges. Then, edge detection was applied on each M-mode image to derive the initial near and far wall boundaries and the rate of change [32]. The snake segmentation system [6] was also used to refine the derived snake contours [see Fig. 4(e)] found on the M-mode image. From the derived contours at the far and near wall boundaries of the M-mode image, the diastolic and systolic diameters (plaque–lumen) of the carotid artery were calculated by finding corresponding maxima and minima (and vice versa) at the near and far wall boundaries of the M-mode image and then estimating their difference, which is the diameter rate of change [see Fig. 4(f)]. The extracted contours for the rate of change were averaged to form the final state diagram of the video [see Fig. 4(f), showing final states of the video], where diastolic and systolic frames were estimated at the maxima and minima of the curve.

From the final state diagram of the video in Fig. 4(f), a full cardiac cycle was selected by identifying the starting and ending frames of the cycle. The frames of the video corresponding to the identified cardiac cycle were then extracted. The segmentation algorithm (see Section II-F) was then applied on the frames representing a full cardiac cycle.

H. Evaluation of the Segmentation Method, and State and Strain Metrics

The video segmentation methods were evaluated using the true-positive fraction (TPF) and the true-negative fraction (TNF), corresponding to sensitivity and specificity, respectively [33]. Ratios of overlapping areas, can also be assessed by applying the similarity kappa index, KI, and the overlap index as used in [6]. These indices were computed at each video frame as

$$\mathrm{TPF} = \frac{|AS \cap GT|}{|GT|}, \quad \mathrm{TNF} = \frac{|\overline{AS} \cap \overline{GT}|}{|\overline{GT}|},$$
$$\mathrm{KI} = 2\frac{|GT \cap AS|}{|GT| + |AS|}, \quad \mathrm{overlap} = \frac{|GT \cap AS|}{|GT \cup AS|}, \quad (2)$$
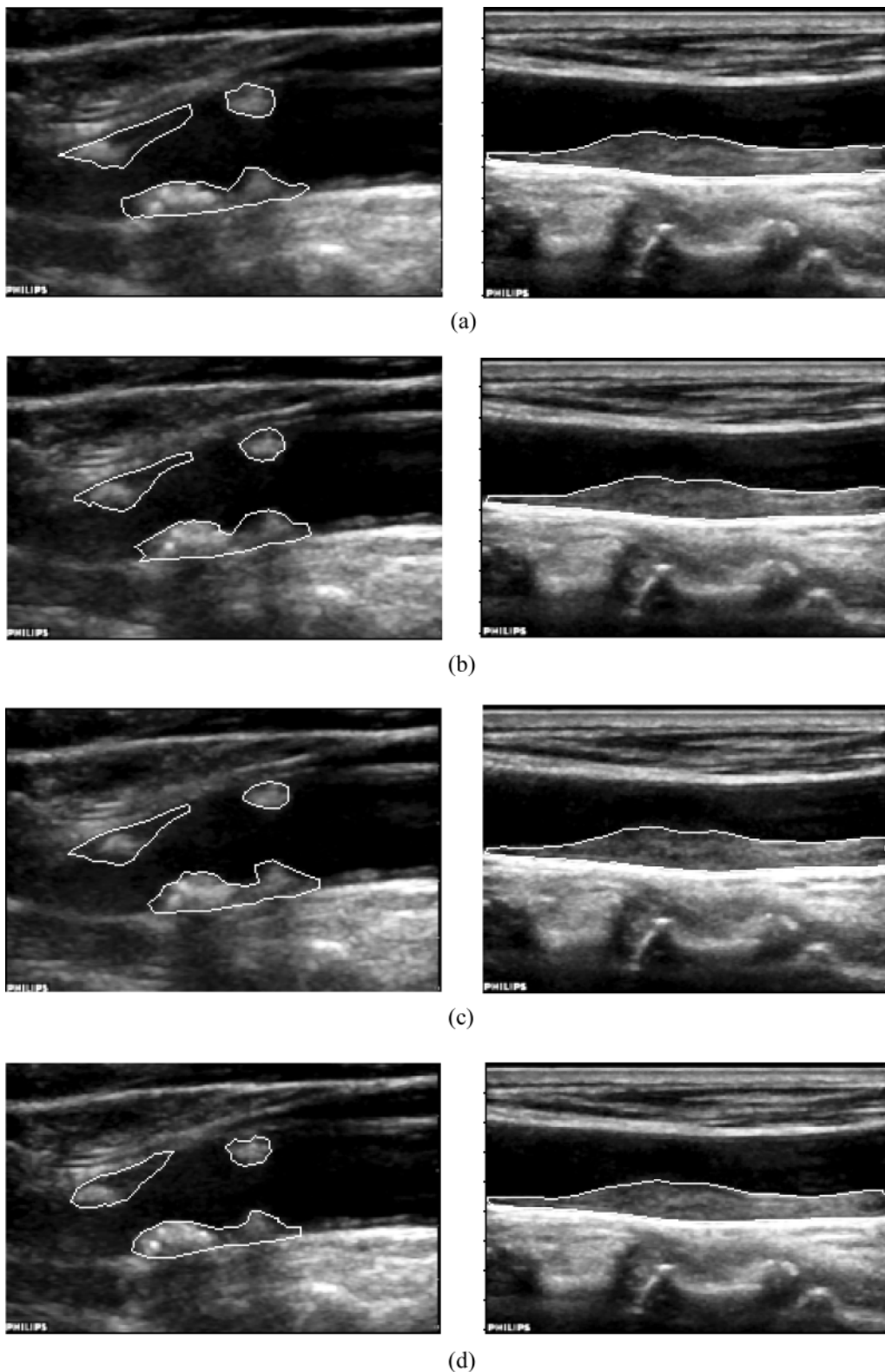
Fig. 3. Two different examples of plaque segmentation of plaques appearing at the CCA in the left and right column, respectively, at the (a) 50th, (b) 60th, (c) 70th, and (d) 150th video frames of the videos.

where $|\ |$ denotes the total number of pixels within the enclosed boundary (or cardinality, which is the number of elements in the set), $\bigcap$ denotes the intersection (the number of common pixels in the manual and snake-segmented areas), and $\bigcup$ the union (the number of all pixels defined by the manual and snake-segmented areas, where the common pixels are considered only once). GT denotes the number of pixels defined by the segmented area, representing ground truth delineated by the expert, and $\overline{\text{GT}}$ its complement. AS denotes the number of pixels belonging
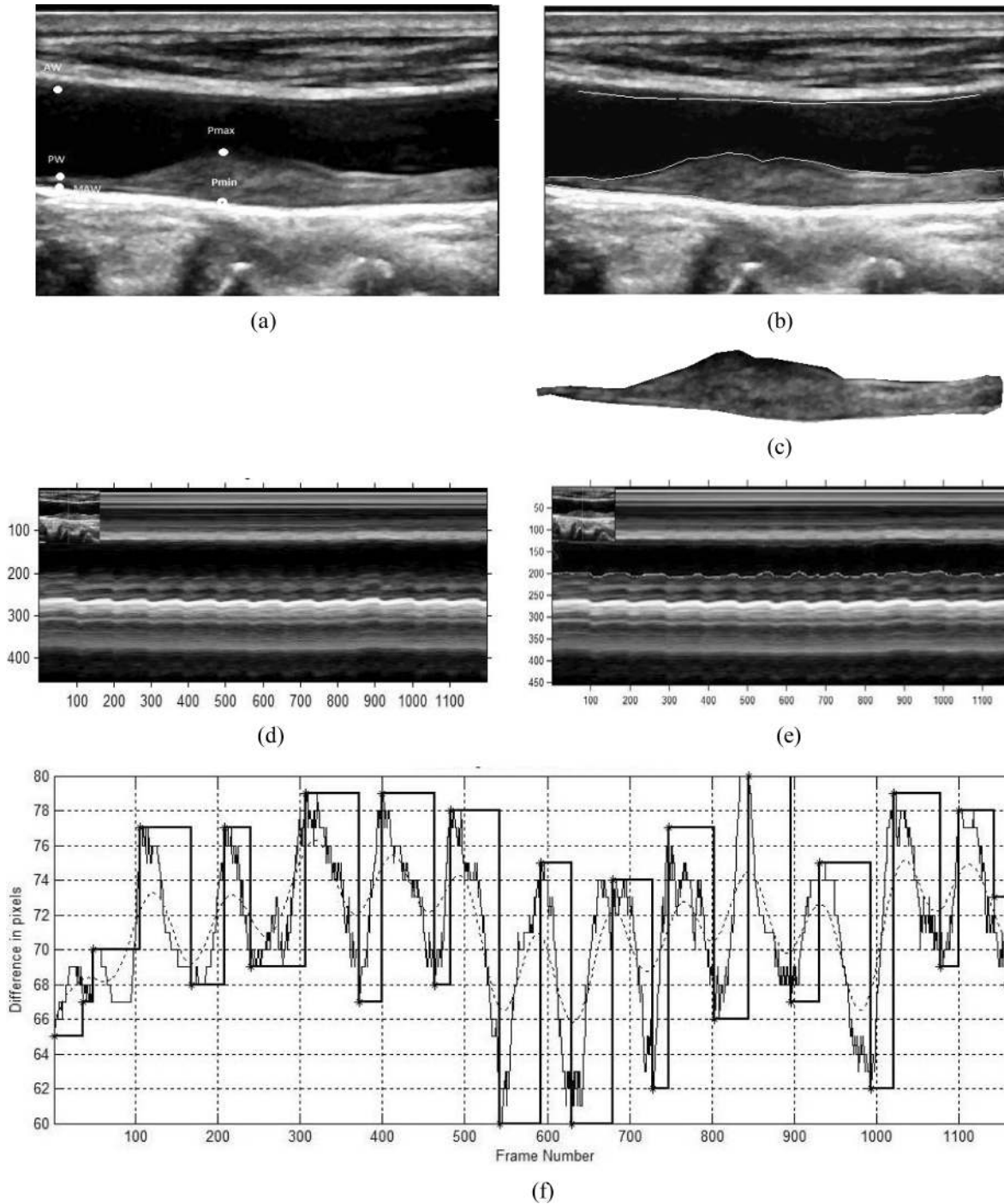
Fig. 4. Illustration of the M-mode generation (see Section II-G for the implementation details), (a) first normalized and despeckled (with DsFlsmv) frame of a B-mode ultrasound video of the CA, (b) segmentation of the plaque boundaries and the near wall of the CA by snakes, (c) extracted plaque, (d) despeckled M-mode image generated from the CA video for a selected B-mode line, (e) initial M-mode states superimposed on the original M-mode image at the far and near walls respectively, (f) diameter change (averaged across the major plaque axis quintiles, with step diagram and systolic and diastolic frames of the video with maximum carotid diameter during distension (*) and maximum carotid diameter during contraction. Diastolic and systolic frames (from 0–1200) (100 frames per second = 12 seconds). Contraction frames: 1, 36, 168, 240, 372, 464, 543, 629, 728, 803, 896, 993; Distension frames: 49, 106, 208, 306, 400, 483, 592, 680, 747, 844, 931; Minimum carotid diameter: 2mm at frame 543; Maximum carotid diameter: 2.67 mm at frame 844. In (a), we illustrate the points adventitia wall (AW), plaque wall (PW), media-adventitia wall (MAW), plaque at maximum point (P_{max}), and plaque at minimum point (P_{min}) (see [34] for definition).

in the area obtained by the snake segmentation method, and $\overline{AS}$ its complement. The intersection gives the probability that both AS and GT occur and the union is the probability that either AS or GT occurs.

To further evaluate the state-based identification algorithm, the following metrics between the automated and the manual state diagram timings were computed for each subject (video).

The root mean square error (RMSE):

$$\text{RMSE} = \sqrt{\sum_i |A_i - M_i|^2}/N, \tag{3}$$

where i represents the frame number, A and M represent the automated and manual state diagrams, and N is the number of states ($2\times$ the heart rhythm).

The normalized mean square error (NMSE):

$$NMSE = 100 * \text{RMSE}/\text{std}_N, \tag{4}$$

where std_N is the standard deviation over one subject (or video), which can be calculated as the root of the mean variance.

The mean average error (MAE) is

$$\text{MAE} = \sum_i |A_i - M_i|/N. \tag{5}$$

The mean average relative error is

$$\text{MARE} = \sum_i \left| \frac{A_i - M_i}{M_i} \right|/N. \tag{6}$$

The carotid diameter during contraction (CDC) and the carotid diameter during distension (CDD), and the percentage of the carotid wall distension (%CWD):

$$\%\text{CWD} = \frac{\text{CDD} - \text{CDC}}{\text{CDC}} * 100. \tag{7}$$

The radial and longitudinal movements in these videos have been also investigated, where regions of interest (ROIs) were selected for each CCA video [see Fig. 4(a)] on the first normalized despeckled frame [34]. More specifically, three ROIs, namely, the adventitia wall (AW) at the near wall, the plaque wall (PW), and the media-adventitia wall (MAW), were selected at the far wall of the CCA, and two ROIs, namely, the maximum plaque border ($P_{\max}$) and the minimum plaque border ($P_{\min}$) were selected. The following equations were used to calculate the radial (RS), longitudinal (LS), and shear strains (SS) from the radial and longitudinal displacement indices as documented in [34]:

$$\text{RS} = \frac{|\text{RP}_1 - \text{RP}_{1(\text{ed})}| - |\text{RP}_2 - \text{RP}_{2(\text{ed})}|}{\text{RP}_{1(\text{ed})} - \text{RP}_{2(\text{ed})}} \tag{8}$$

$$\text{LS} = \frac{|\text{LP}_1 - \text{LP}_{1(\text{ed})}| - |\text{LP}_2 - \text{LP}_{2(\text{ed})}|}{\text{LP}_{1(\text{ed})} - \text{LP}_{2(\text{ed})}} \tag{9}$$

$$\text{SS} = \arctan\left(\frac{(\text{LP}_1 - \text{LP}_{1(\text{ed})}) - (\text{LP}_2 - \text{LP}_{2(\text{ed})})}{(\text{RP}_{1(\text{ed})} - \text{RP}_{2(\text{ed})})} \right), \tag{10}$$

where RP and LP denote radial and longitudinal displacements, respectively, for a pair of ROIs, and (ed) corresponds to end diastole. Based on (8)–(10), the radial strain at wall (RS), the longitudinal strain (LS), and the shear strain (SS) were calculated.

III. Results

A. Examples of Plaque Video Segmentation

Fig. 3 presents two different examples of video plaque segmentation with atherosclerotic plaques appearing at the CCA in the left and right column. The segmentations were performed for the first and second cardiac cycle, for the 50th, 60th, 70th, and 150th video frames of the video. In the left column, a case from a 61-year-old female asymptomatic subject is presented with three different plaques at the near and far wall of the CCA, with a left CCA stenosis of 35% to 40%. In the right column, one can see a case from a 64-year-old male symptomatic subject with a stent on the right CCA and with a stenosis of 40% to 50%. It is observed that the proposed segmentation algorithm is able to follow the plaque borders consistently as a result of the initialization procedures followed.

B. Evaluation of the Plaque Segmentation Method

Table II tabulates the quantitative results of the statistical analysis based on TNF, TPF, KI, and overlap index for the proposed video segmentation method performed for 1 to 2 cardiac cycles, on 43 ultrasound videos of the CCA for the two different initialization methods (see two last rows in Table II). The results of the automated segmentation method are compared with the manual tracings of the expert, which are considered to be the ground truth. The results show that the proposed method using the two different initialization methods (mean $\pm$ std method 1 and mean $\pm$ std method 2) agrees with the expert by correctly detecting no plaque (TNF) in ($83.7 \pm 7.6\%$ and $84.3 \pm 7.5\%$) of the cases and by correctly detecting a plaque (TPF) in ($85.42 \pm 8.1\%$ and $86.1 \pm 8.0\%$) of the cases. The similarity kappa index, KI, and the overlap index for the proposed video snake segmentation method were equal to 84.6% and 85.3% and 74.7% and 75.4% using the two different initialization techniques, respectively. There was no significant difference between the two methods for all metrics investigated using a pair t-test at $p < 0.05$. However, a small improvement was observed in almost all evaluation metrics when the segmentations were performed with the second initialization method. It should further be noted that the snake contour may be attracted occasionally to local minima and converge to a wrong location. This occurred in less than 10% of the cases (i.e., in 4 videos).

C. M-Mode Generation and State Identification

Fig. 4(e) presents the M-mode image of the video, where the video states are superimposed at the far and near wall, respectively. The insert on the left upper side of the images in Figs. 4(d) and 4(e) indicates the straight perpendicular line that can also be selected by the user of the proposed system to generate the M-mode image. Finally, in Fig. 4(f), the diameter change is presented

TABLE II. PERFORMANCE METRICS OF SENSITIVITY (TRUE-POSITIVE FRACTION, TPF), SPECIFICITY (TRUE-NEGATIVE FRACTION, TNF),
KAPPA INDEX (KI), AND OVERLAP INDEX FOR THE VIDEO SEGMENTATION METHODS PERFORMED ON 43 ULTRASOUND VIDEOS
OF THE CCA FOR THE TWO DIFFERENT INITIALIZATION METHODS.

Segmentation method	Ultrasound data	Sensitivity (TPF)	Specificity (TNF)	KI	Overlap index
Loizou [6]	Images ($N = 80$)	82.7%	80.9%	80.7%	69.3%
Golemati [22]	Images ($N = 4$)	$97.5 \pm 1.0\%$	$96 \pm 10\%$	—	—
Destrempes [7]	Videos (N = 33)	$83.7 \pm 8.3\%$	$94.1 \pm 4.2\%$	0.85 ± 0.75	0.75 ± 0.1
Present study (intensity based initialization)	Videos ($N = 43$)	$85.4 \pm 8.1\%$	$83.7 \pm 7.6\%$	84.6%	74.7%
Present study (initial contour based initialization)	Videos ($N = 43$)	$86.1 \pm 8.0\%$	$84.3 \pm 7.5\%$	85.3%	75.4%

Manual segmentations performed by an expert were used.

with the help of a step diagram showing systolic (1, 36, 168, 240, 372, 464, 543, 629, 728, 803, 896, and 993) and diastolic frames (49, 106, 208, 306, 400, 483, 592, 680, 747, 844, and 931) of the video. The maximum carotid diameter during distension (2 mm at frame 543 indicated with an asterisk) and maximum carotid diameter during contraction (2.67 mm at frame 844 indicated with an asterisk) are also shown.

Table III presents the results of the evaluation metrics between the manual and the automated state diagrams (mean ± std) in microseconds for the asymptomatic and the symptomatic subjects. The RMSE, NRMSE, MAE, and the MARE were for all videos 125.41 ± 11.77 µs, 121.16 ± 10.38 µs, 119.06 ± 11.96 µs, and 5.43 ± 0.95 µs, respectively. The *t*-test test gave statistically significant differences between the asymptomatic and symptomatic cases for all evaluation metrics tabulated in Table III.

Table IV illustrates the results of the CDC, CDD, and the %CWD for the asymptomatic and the symptomatic subjects (mean ± std). The CDC, CDD, and the %CWD for the asymptomatic and the symptomatic groups were 5.13 ± 0.34 and 5.48 ± 0.29 mm, 5.89 ± 0.31 and 6.27 ± 0.35 mm, and 10.2 ± 1.03 and $16.09 \pm 0.83\%$, respectively. The *t*-test, shown in the last row of Table IV, performed between the values obtained for the asymptomatic and symptomatic cases at $p < 0.05$ gave no statistically significant differences between them.

D. Strain Metrics

Table V presents the strain indices (mean ± std) over two consecutive cardiac cycles for the asymptomatic and symptomatic groups. More specifically, the following measures were evaluated, a radial strain at wall (RSW) of $5.13 \pm 0.34\%$, a longitudinal strain of $2.84 \pm 0.65\%$, a shear strain at wall (SSW) of 0.42 ± 0.12 rad, a shear strain at plaque (SSP) of 0.06 ± 0.01 rad, and a radial strain at

plaque (RSP) of 3.13 ± 1.21 rad. All strain indices between the asymptomatic and symptomatic subjects were found to be not significantly different.

IV. DISCUSSION

The results of the proposed integrated video segmentation method can be favorably compared with the results of the segmentation of the carotid plaque in ultrasound images presented in [6], and also with the results presented in [7] and [22] (see also Table II). Comparing the proposed video segmentation method with the one presented in [6], one may observe that the TNF, TPF, KI, and overlap index are larger in this study. This may be attributed to the fact that the videos used here were of better quality than the images used in [6]. The results reported in [22] are better than the ones reported in [6] and in this study, but it should also be taken into consideration that the number of images used in [22] was very small (only 4 ultrasound images of the CCA) when compared with the study in [6] and [7], in which 80 and 33 videos were used, respectively. Furthermore, in [7], where video segmentation of atherosclerotic carotid plaque in 33 video sequences was proposed, similar results were obtained for the KI and overlap index (see also Table II). Also, the specificity was $94.1 \pm 4.2\%$ in [7] versus $84.3 \pm 7.5\%$ here. It should also be noted that the standard deviations obtained for the presented work are larger than the ones obtained in [7].

The results of Table III show that all error measurements (RMSE, NRMSE, MAE, and MARE) calculated in this study are much smaller, with much smaller standard deviations, than the ones obtained in a recent study [32] in which M-mode state based identification in 10 CCA videos was investigated. The smaller deviations obtained in this study could be attributed to the fact that a heterogeneous group of videos was investigated in [32].

TABLE III. MEAN ± STD EVALUATION METRICS BETWEEN THE MANUAL AND THE AUTOMATIC STATES IN MICROSECONDS.

Video	RMSE	NRMSE	MAE	MARE
Asymptomatic ($N = 38$)	191.25 ± 13.31	212.79 ± 12.42	182.63 ± 19.76	7.12 ± 1.01
Symptomatic ($N = 5$)	59.56 ± 10.23	43.53 ± 8.34	55.50 ± 4.20	3.74 ± 0.89
t-test between asymptomatic and symptomatic[1]	S ($p = 0.04$)	S ($p = 0.002$)	S ($p = 0.031$)	S ($p = 0.029$)

RMSE = relative mean square error; NRMSE = normalized mean square error; MAE = mean absolute error; MARE = mean absolute relative error.

[1]Test carried out at $p < 0.05$; S = significantly different.

TABLE IV. Mean ± Std Carotid Diameter During Contraction (CDC) in Millimeters, Carotid Diameter During Distension (CDD) in Millimeters, and Percent of Carotid Wall Distension (%CWD) for the Automated Segmentations.

Video	CDC (mm)	CDD (mm)	%CWD
Asymptomatic ($N = 38$)	5.13 ± 0.34	5.89 ± 0.31	10.2 ± 1.03
Symptomatic ($N = 5$)	5.48 ± 0.29	6.27 ± 0.35	16.09 ± 0.83
t-test between asymptomatic and symptomatic[1]	NS ($p = 0.59$)	NS ($p = 0.11$)	NS ($p = 0.38$)

[1]Test carried out at $p < 0.05$. NS = not significantly different.

The results of Table IV are also consistent with [32] (CDC = 5.26 ± 0.52 mm, CDD = 5.81 ± 0.59 mm, %CWD = $10.32 \pm 4.71\%$), in which M-mode state-based identification in 10 ultrasound videos of the CCA was performed.

Strain indices, similar to the ones reported in Table V, were also estimated for asymptomatic and symptomatic subjects in [34] (RSW = $5.50 \pm 2.90\%$, LS = $2.15 \pm 1.36\%$, SSW = 0.37 ± 0.20 rad, SSP = 0.10 ± 0.07 rad, and RSR = 4.32 ± 2.34 rad for the asymptomatic and RSW = $5.09 \pm 1.73\%$, LS = $2.79 \pm 1.71\%$, SSW = 0.39 ± 0.18 rad, SSP = 0.07 ± 0.04 rad, and RSR = 3.33 ± 1.82 rad for the symptomatic subjects) to quantify the mechanical behavior of the CCA artery in the radial and longitudinal directions. More specifically, four different motion estimation techniques of the CCA in ultrasound videos were investigated and applied on synthetic videos with known properties. It was also shown in [34], as can be seen by the presented results, that the errors were higher in the longitudinal direction than in the radial. No statistically significant differences were found for all indices between the asymptomatic and symptomatic subjects in [34] or in the present study.

In [21] and [22], in which image segmentation of the atherosclerotic carotid plaque was performed, images were neither normalized nor despeckled, nor was an automatic contour estimation used as in this study. The video normalization method presented in this study ensures that the segmentation method and the results are not dependent on the equipment used. This is not the case for the video segmentation method proposed in [7], in which the region-based segmentation was established using the statistical distribution of the gray level of the frames and speckle noise was not taken into consideration. Furthermore, the results of this study showed that the proposed video segmentation method performs very closely to the method for atherosclerotic plaque segmentation presented in [6]. The presented work can also be favorably compared with the recent video segmentation study in [7], performed on 33 subjects (see also Table II).

A. Plaque Contour Initialization

The key point of the proposed framework is the accuracy of the initialization. Two different methods were investigated in this work for initial contour estimation. However, both methods gave similar segmentation evaluation performance. There was no significant difference for all evaluation metrics investigated. In [7], the method for video segmentation proposed was also semiautomatic, in the sense that it required an initial manual segmentation of the plaque in the first frame, and then proceeded to the segmentation of the entire sequence without further user interaction. In [21] and [22], the initialization of the segmentation algorithm was performed automatically based on the echogenicity of the lumen and the plaque, or the Hough transform, respectively. These methods were tested on image sequences, but were processed individually. In the presented methodology it was assumed that if the method performed satisfactorily for an individual image, it might also perform well for a whole sequence of images, with each image processed individually. However, a more sophisticated tracking procedure, taking into consideration the interrelations between neighboring frames by utilization of motion estimation, could be taken into consideration in future work. Such a method could achieve automated video segmentation with even less manual intervention.

Initial contour estimation for segmenting ultrasound images was also proposed in [35], derived from the polar image by combining information extracted from the probability function of the contour position, and more specifically from the function maximum location and the first zero crossing of its derivative. Then, starting from the initial contour, a region of interest was automatically selected and the process iterated until the snake contour

TABLE V. Mean ± Std Values of Strain Indices of the Carotid Artery for Asymptomatic ($N = 38$) and Symptomatic ($N = 5$) Subjects Over Two Consecutive Cardiac Cycles.

Strain indices	Asymptomatic ($n = 38$)	Symptomatic ($n = 5$)	t-test[1]
RSW (%)	5.13 ± 0.34	5.37 ± 0.26	NS (0.31)
LS (%)	2.84 ± 0.65	2.97 ± 0.42	NS (0.72)
SSW (rad)	0.42 ± 0.12	0.49 ± 0.17	NS (0.43)
SSP (rad)	0.06 ± 0.01	0.12 ± 0.03	NS (0.096)
RSP (rad)	3.13 ± 1.21	3.9 ± 0.98	NS (0.59)

RSW = radial strain at wall; LS = longitudinal strain at wall; SSW = shear strain at wall; SSP = shear strain at plaque; RSP = radial strain at plaque.
[1]Test carried out at $p < 0.05$, NS = not significantly different.

evolution could be ignored. In [36], a cost function was calculated and used as an input to the image plaque segmentation algorithm. In [19], a dynamic balloon model [18] represented by a triangular mesh was applied for detecting the plaque borders on two 3-D ultrasound carotid images for which the initial contour was placed manually. In all of these studies and in the present study, the significance of the initial contour placement was not exhaustively investigated to estimate how this influences the final segmentation result.

B. Video States Identification

By identifying the states of the CCA, the normal and abnormal plaque motion can be investigated. It was shown in [7] and [31], and in the present study, that M-mode state-based modeling derived from B-mode videos can be used successfully to derive the carotid states and assess the corresponding wall changes. This work also shows that state-based video modeling can be used to identify video segments' dynamic behavior in ultrasound videos of the CCA. However, further work is needed for validating the proposed method and for differentiation between normal and abnormal state-based plaque motion analysis.

There are several studies reported in the literature, in which state-based identification of the CCA was performed. More specifically, Golemati *et al.* [22], used block-matching-based techniques to estimate arterial motion from B-mode CCA ultrasound images. They found that arterial wall distensibility in the radial direction was significantly higher than distensibility in the longitudinal direction ($10.2 \pm 4.5\%$ versus $2.5 \pm 0.89\%$). In another study [34], the same group performed a comparison of block-matching differential methods for motion analysis of the CCA in ultrasound videos. Their results were very similar with the ones presented here (see Table V), but a slightly different distensibility of $13.15 \pm 0.93\%$ in the radial direction (see Table IV). Differences could be easily attributed to the nature of the different video data sets investigated.

In [37], it was shown that M-mode ultrasound analysis can be a sensitive tool for measurements of strain decrease with increasing age and male sex and strain increase with smoking and obesity when evaluated on the right CCA. Therefore, it might be used for screening of unsuccessful vascular aging and still potentially reversible subclinical carotid atherosclerosis, thereby lowering the cut-off value of vascular damage toward the values of unaffected population. It provides opportunities for introduction of different therapeutic or life-style change strategies for reduction or retardation of overt clinical manifestation of cerebrovascular disease.

In [31], the states of echocardiogram videos were identified based on a state classifier detector, which first detects the view boundaries using histogram-based comparison and edge change ratio. The accuracy of the classifier was 97.19%, which was higher than two existing approaches

[38], [39]. Misclassification error of state detection was less than 13%, which is reasonably low.

Future research perspectives may be orientated toward to the development of new M-mode identification algorithms, and motion field of the arterial wall. Further, the separation between healthy and diseased arterial wall remains to be studied in detail.

C. Limitations of the Video Segmentation Method

There are some limitations in the proposed methodology that are summarized below. Cases of plaque type I and type V [6], [25], [26] (see Section II-B) were not considered for segmentation. If the plaque is of type I, borders are not clearly visible. Plaques of type V produce acoustic shadowing and the plaque is also not clearly visible [25]. However, there are also inherent difficulties for segmentation of the carotid videos and the corresponding plaques that arise not only from the use of different protocols but also because of differences in anatomy as well as the extent of the atherosclerosis and plaque presence. The presence of extensive and severe carotid stenosis may cause the initialization to completely fail because there will be difficulty in establishing the lumen. In addition, the presence of extensive plaques in the near wall may cause inaccurate segmentation of the far-wall adventitia. It should be noted that the parameters for each processing step (for example, the size of the moving pixel window, the number of iterations, the number of frames for which the contour was reinitialized) were selected for maximum performance. However, there were about 10% of the cases where the final snake contour did not converge properly.

The average computation time for the snake contour was about 9 s per frame, using a Pentium III (Intel Corp., Santa Clara, CA) desktop computer with 3.2 GHz of RAM memory, whereas in [7] it was 30 s per frame. It is noted that the expert clinician required more than 25 s per frame for the manual delineation. An average processing time of 20 s per image in case of the segmentation of the CCA images is reported in [21, p. 1267, end of Section II], whereas in [7], the average processing time per image was 30 s. It should also be noted that the accuracy of the proposed method has been further improved (see last two rows of Table II) when the first frame of the video was initialized with the second initialization method proposed in this study (see Section II-E).

Further efficiency can be achieved in a commercial version, in which the proposed algorithm may be designed to perform in parallel with the clinician's evaluation, so the clinician might carry on with the patient examination while the segmentation of the whole sequence is performed. Thus, there is a reasonable expectation that a clinically applicable version will be created in the future. Further improvement could be achieved to enable the use of the proposed video segmentation technique in the real clinical practice if the initialization of the snake contours (see Section II-E) is applied every 30 or 40 frames so that

the snake contour is repositioned closer to the plaque borders.

In everyday clinical practice, the ultrasonographer manipulates the transducer and mentally transforms the 2-D images into anatomical volume, or structure, or lesion, to make a diagnosis. Three-dimensional ultrasound attempts to provide the ultrasonographer with a more realistic reconstruction and visualization of the 3-D structure under investigation, thus overcoming the limitations of 2-D imaging, reducing the variability of assessment and aiding in improved diagnosis. The additional information may also enable evaluation of changes in the volume but also in the surface morphology, providing additional information for stroke risk analysis [23]. The use of 3-D techniques has primarily focused on measuring volume changes through time to monitor disease progression [40]– [42]. Landry *et al.* [40] demonstrated that plaque volume change can be reliably measured using 3-D ultrasound. They showed that a 20% to 35% change can be measured with 95% confidence for plaques of volume <100 mm^3. For larger plaques (volume >100 mm^3), with 95% confidence, they showed that we can measure finer changes of the order of 10% to 20%, respectively. Chiu *et al.* [41] developed a 3-D segmentation method for measuring the combined thickness of the plaque, the intima, and media (vessel wall plus plaque thickness or VWT). The authors proposed the use of 3-D VWT and VWT-change maps for identifying disease progression in relations to disturbances of flow. The authors extended their work in [42], in which they measured VWT volume changes for assessing and monitoring carotid artery disease.

V. Concluding Remarks

The method presented in this study proposes an integrated system for the segmentation of atherosclerotic carotid plaque in longitudinal ultrasound image sequences. The method integrates video frame normalization, despeckling, and accurate segmentation using active contours. Such a system can reduce the time required for the video analysis, and also the subjectivity that accompanies manual delineations and measurements. The method will be further evaluated on a larger number of ultrasound videos and with ground truth from multiple experts. Future work will focus on improving the segmentation procedure, such that it can satisfactorily process special plaque cases and difficult-to-segment videos, taking into consideration, for example, a statistical approach to initialize and teach the snake about the blood flow and plaque area [37], as was also investigated in [6]. Furthermore, the segmentation system proposed in this study will be incorporated into a computer-aided diagnostic system that supports the texture analysis of the segmented plaque, as documented in [43] and [44], providing an automated system for the early diagnosis and the assessment of the risk of stroke. It will also be of great interest to measure the transversal as well the longitudinal movements at the two arterial sides of

the CCA (left and right CCA) to find differences between the two sides. Another interesting application would be to investigate the longitudinal movement of the arterial wall, as in [45], but also apply the aforementioned technique at different arterial sides that are known to be susceptible to the atherosclerosis disease, such as the carotid bifurcation and proximal internal carotid artery. Furthermore, the integrated plaque video segmentation method proposed will greatly facilitate the automated plaque motion analysis [34], [46]. Finally, it can be seen that an optimized implementation based on parallelization could provide close to real-time video processing.

Appendix A
Supplementary Material on the Two Segmentation Initialization Methods

The first initialization method for establishing the positioning of the initial snake contour uses intensity information, morphological operations, and edge detection to find the initial outline of the plaque. The steps of the first initialization procedure are described in what follows and can also be seen in Fig. 1. To begin, the normalized and despeckled first video frame of the cardiac cycle is thresholded—the threshold is calculated from the despeckled grayscale image frame according to Otsu's method and the corresponding normalization [26]. Pixels that have smaller intensity values than this threshold are set to zero, whereas pixels with larger intensity values are set to one, resulting in a binary image [see Fig. 1(c)]. The binary image is dilated [see Fig. 1(c)]. Here, a square window shape structuring element with a size of 9 × 9 pixels (0.53 × 0.53 mm) was applied to the binary image frame. This morphological operation is performed to close small gaps and form a continuous boundary. On the dilated area, erroneous small edges that might trap the snake must be removed. This is carried out by labeling connecting components in the image, where the number of connecting components was chosen to be eight. Small segments that have an area less than 20 pixels (1.2 mm), and do not belong in the boundary are therefore removed [see Fig. 1(c)]. It should be noted that the choice of the square window structuring element and the number of connected components was chosen after several experiments made using the guidance of the expert neurologist (coauthor M. Pantziaris). Next, the contour matrix of the remaining objects is extracted [see Fig. 1(d)], which should represent the lumen and the near and far carotid wall boundaries. The areas of interest in the image, where the plaque will be detected are manually selected [via the positioning of an ROI in the first video frame, see Fig. 1(e)], and the contour matrix of the corresponding regions is extracted by locating points and their coordinates on the plaque borders (plaque–lumen boundary, contour). To form the initial plaque–adventitia boundary contour, the two far ends of the contour matrix are connected together. Interpolating B-splines are used to smooth the corresponding

boundaries [see Fig. 1(f)] and these smoothed boundaries are sampled in 30 equal segments. The 30 sampled points are the ones used to initialize the active contours plaque segmentation. In a case in which there are multiple plaques in the CCA [see Figs. 3(a)–3(d)] the selection of the plaque could be repeated manually by placing a different area of interest, and the procedure could be performed for each plaque independently.

The second initialization method for establishing the positioning of the initial snake contour is based on the use of active contours without edges [13] by Chan and Vese and can be seen in Fig. 2. We use in Fig. 2 the same image as in Fig. 1(a) so that direct comparisons can be made between the two initialization methods. Level-set methods [47] work in several spatial dimensions, but more importantly they can handle topological changes naturally. Using the level-set formulation of the active contours without edges by Chan and Vese [13] (Chan–Vese model), the regions corresponding to the lumen and the carotid wall (including the plaque) can be automatically segmented. It is also noted that the Chan–Vese formulation can use the corresponding energy terms used in the snake formulation.

The Chan–Vese model [13] corresponds to a region-based level-set method which uses the Mumford–Shah functional in the level-set framework for a piecewise constant representation of an image. The evolution of the curve is governed by properties of the region of the image $u_0(x,y)$ enclosed by the curve. The model tries to separate the image into regions based on pixel intensities and introduces the following energy functional:

$$
\begin{aligned}
F(c_1, c_1, C) = {} & \mu \cdot \text{Length}(C) + \nu \cdot \text{Area}(\text{inside}(C)) \\
& + \lambda_1 \int\limits_{\text{inside}(C)} |u_0(x,y) - c_1|^2 \mathrm{d}x\mathrm{d}y \\
& + \lambda_2 \int\limits_{\text{outside}(C)} |u_0(x,y) - c_2|^2 \mathrm{d}x\mathrm{d}y,
\end{aligned}
$$

$$(A.1)$$

where $\mu \geq 0$, $\nu \geq 0$, and $\lambda_1, \lambda_2 > 0$ are fixed parameters.

Without loss of generality, the initialization contour is a disk with radius of 2.1 mm randomly placed in the image background (segmented from simple thresholding with a threshold close to zero). For the evaluation of the level-set segmentation, in addition to downsampling the original ultrasound image frame by a factor of 4 to accelerate the segmentation, the values of the different parameters used are $\mu = 0.2$; h, the space step, is set to 1; and Δt, the time step, is set to 0.25. For computation of the regularized versions of H and δ_0, $\varepsilon = 1$, as used in [13]. The values for the different parameters for the Chan–Vese model were empirically verified. The empirical verification also showed that slight variation in the value of the parameters would not have a significant effect on the final segmentation. The first two terms in (A.1) control the regularity by penalizing the length and the enclosed area of C. The choice of $\mu = 0.2$ allows the segmentation to accurately match the data, while still resulting in a relatively smooth

curve. The term ν provides a penalty on the foreground area resulting from the segmentation, and here is set to 0. For segmenting the lumen and the adventitia, the energy contributed by the intensity variance of the two regions is equally weighted to $\lambda_1 = \lambda_2 = 1$. In a large number of applications [13], including this implementation, $\lambda_1 = \lambda_2 = 1$ and $\nu = 0$; however, parameters of the energy functional may need to be modified if new smoothness constraints are needed or if data sets with different visual quality are used [49].

The Chan–Vese model is first applied to the normalized, despeckled first video frame. To initialize the active contours without edges, a rough outline of the lumen is used, resulting in faster convergence. This outline is found by incorporating clinical and image intensity information. According to the clinical guidelines, the lumen should be imaged longitudinally around the middle of the frame, and following normalization it has a limited range of intensity values. Thus, after thresholding the despeckled, normalized first video frame, for intensities less than 4 (which is below the maximum of the lumen intensity value after normalization [25]) and morphological opening with a circular element of 0.3×0.3 mm to close any holes, the largest region in the middle of the frame corresponds to a roughly segmented lumen [see Fig. 2(b)]. The outline of this rough segmentation is used to initialize the Chan–Vese model. Figs. 2(c) and 2(d) present the Chan–Vese model segmentation, showing only the outline at the far and near wall including the plaque of the CCA, respectively. The final result of the Chan–Vese model is shown in Fig. 2(e). Next, the region corresponding to the lumen is eroded using a circular element of 0.82×0.82 mm to ensure that the boundaries that will be used for initialising the final segmentation will be in the lumen but outside the carotid wall. This segmentation provides initialization of boundaries of the near and far wall of the carotid. These boundaries are sampled and 30 equally spaced sampled points are used to initialize the active contours for atherosclerotic carotid plaque segmentation [see Fig. 2(e)]. The boundaries area across the entire length of the wall will include all plaques present.

REFERENCES

[1] W. E. Hellings, W. Peeters, F. L. Moll, S. R. Piers, J. van Setten, P. J. Van der Spek, J. P. de Vries, K. A. Seldenrijk, P. C. De Bruin, A. Vink, E. Velema, D. P. de Kleijn, and G. Pasterkamp, "Composition of carotid atherosclerotic plaque is associated with cardiovascular outcome: A prognostic study," *Circulation*, vol. 121, no. 17, pp. 1941–1950, May 2010.
[2] C. Schmitt, G. Soulez, R. L. Maurice, M.-F. Giroux, and G. Cloutier, "Noninvasive vascular elastography: Toward a complementary characterization tool of atherosclerosis in carotid arteries," *Ultrasound Med. Biol.*, vol. 33, no. 12, pp. 1841–1858, 2007.
[3] I. M. Graf, J. Su, D. Yeager, J. Amirian, R. Smalling, and S. Emelianov, "Methodical study on plaque characterization using integrated vascular ultrasound, strain and spectroscopic photoacoustic imaging," in *Proc. SPIE*, 2011, vol. 7899, art. no. 789902.
[4] H. Ribbers, R. G. P. Lopata, S. Holewijn, G. Pasterkamp, J. D. Blankensteijn, and C. L. de Korte, "Noninvasive two-dimensional strain imaging of arteries: Validation in phantoms and preliminary

experience in carotid arteries in vivo," *Ultrasound Med. Biol.*, vol. 33, no. 4, pp. 530–540, 2007.

[5] H. Shi, C. C. Mitchell, M. McCormick, M. A. Kliewer, R. J. Dempsey, and T. Varghese, "Preliminary in vivo atherosclerotic carotid plaque characterization using the accumulated axial strain and relative lateral shift strain indices," *Phys. Med. Biol.*, vol. 53, no. 22, pp. 6377–6394, 2008.

[6] C. P. Loizou, C. S. Pattichis, M. Pantziaris, and A. N. Nicolaides, "An integrated system for the segmentation of atherosclerotic carotid plaque," *IEEE Trans. Inf. Technol. Biomed.*, vol. 11, no. 6, pp. 661–667, Nov. 2007.

[7] F. Destrempes, J. Meunier, M.-F. Giroux, G. Soulez, and G. Cloutier, "Segmentation of plaques in sequences of ultrasonic B-mode images of carotid based on motion estimation and a Bayesian model," *IEEE Trans. Biomed. Eng.*, vol. 58, no. 8, pp. 2202–2211, 2011.

[8] J. F. Polak, M. J. Pencina, D. H. O'Leary, and R. B. D'Agostino, "Common-carotid artery intima-media thickness progression as a predictor of stroke in multi-ethnic study of atherosclerosis," *Stroke*, vol. 42, no. 11, pp. 3017–3021, 2011.

[9] Q. Liang, I. Wendelhag, J. Wikstrand, and T. Gustavsson, "A multiscale dynamic programming procedure for boundary detection in ultrasonic artery images," *IEEE Trans. Med. Imaging*, vol. 19, no. 2, pp. 127–142, Feb. 2000.

[10] S. Petroudi, C. P. Loizou, M. Pantziaris, and C. S. Pattichis, "Segmentation of the common carotid intima-media complex in ultrasound images using active contours," *IEEE Trans. Biomed. Eng.*, vol. 59, no. 11, pp. 3060–3069, Nov. 2012.

[11] D. Kashiwazaki, T. Yoshimoto, T. Mikami, M. Muraki, S. Fujimoto, K. Abiko, and S. Kaneko, "Identification of high-risk carotid artery stenosis: Motion of intraplaque contents detected using B-mode ultrasonography," *J. Neurosurg.*, vol. 117, no. 3, pp. 574–578, 2012.

[12] C. P. Loizou, C. S. Pattichis, S. Petroudi, M. Pantziaris, T. Kasparis, and A. N. Nicolaides, "Segmentation of atherosclerotic carotid plaque in ultrasound video," in 34th *Ann. Int. Conf. IEEE Eng. Med. Biol.*, 2012, art. no. WeA03.2.

[13] T. Chan and L. Vese, "Active contours without edges," *IEEE Trans. Image Process.*, vol. 10, no. 2, pp. 266–277, 2001.

[14] A. Hamou and M. El-Sakka, "A novel segmentation technique for carotid ultrasound images," in *Int. Conf. Acoustic Speech and Signal Processing*, 2004, pp. III-521–III-524.

[15] A. R. Abdel-Dayen and M. R. El-Sakka, "A novel morphological-based carotid artery contour extraction," in *Canadian Conf. Electrical and Computer Engineering*, 2004, vol. 4, pp. 1873–1876.

[16] F. Mao, J. Gill, D. Downey, and A. Fenster, "Segmentation of carotid artery in ultrasound images: Method development and evaluation technique," *Med. Phys.*, vol. 27, no. 8, pp. 1961–1970, Aug. 2000.

[17] P. Abolmaesumi, M. R. Sirouspour, and S. E. Salcudean, "Real-time extraction of carotid artery contours from ultrasound images," in *Proc. IEEE Int. Conf. Computer Based Medical Systems,* 2000, pp. 181–186.

[18] L. D. Cohen, "On active contour models and balloons," *CVGIP Image Underst.*, vol. 53, no. 2, pp. 211–218, 1991.

[19] J. D. Gill, H. M. Ladak, D. A. Steinman, and A. Fenster, "Segmentation of ulcerated plaque: A semi-automatic method for tracking the progression of carotid atherosclerosis," in *World Congr. Medical Physics and Biomedical Engineering*, 2000, pp. 1–4.

[20] D. Williams and M. Shah, "A fast algorithm for active contour and curvature estimation," *GVCIP Image Underst.*, vol. 55, no. 1, pp. 14–26, 1992.

[21] S. Delsanto, F. Molinari, P. Giustetto, W. Liboni, S. Badalamenti, and J. S. Suri, "Characterization of completely user-independent algorithm for carotid artery segmentation in 2D ultrasound images," *IEEE Trans. Instrum. Meas.*, vol. 56, no. 4, pp. 1265–1274, 2007.

[22] S. Golemati, J. Stoitsis, E. G. Sifakis, T. Balkisas, and K. S. Nikita, "Using the Hough transform to segment ultrasound images of longitudinal and transverse sections of the carotid artery," *Ultrasound Med. Biol.*, vol. 33, no. 12, pp. 1918–1932, 2007.

[23] A. Zahalka and A. Fenster, "An automated segmentation method for three-dimensional carotid ultrasound images," *Phys. Med. Biol.*, vol. 46, no. 4, pp. 1321–1342, 2001.

[24] E. Ukwatta, J. Yuan, D. Buchanan, B. Chiu, J. Awad, W. Qiu, G. Parraga, and A. Fenster, "Three-dimensional segmentation of three-dimensional ultrasound carotid atherosclerosis using sparse field level sets," *Med. Phys.*, vol. 40, no. 5, art. no. 052903, 2013.

[25] A. N. Nicolaides, M. Sabetai, S. K. Kakkos, S. Dhanjil, T. Tegos, and J. M. Stevens, "The asymptomatic carotid stenosis and risk of stroke study," *Int. Angiol.*, vol. 22, no. 3, pp. 263–272, 2003.

[26] T. Elatrozy, A. Nicolaides, T. Tegos, A. Zarka, M. Griffin, and M. Sabetai, "The effect of B-mode ultrasonic image standardization of the echodensity of symptomatic and asymptomatic carotid bifurcation plaque," *Int. Angiol.*, vol. 17, no. 3, pp. 179–186, 1998.

[27] J. S. Lee, "Digital image enhancement and noise filtering by using local statistics," *IEEE Trans. Pattern Anal. Mach. Intell.*, vol. 2, no. 2, pp. 165–168, 1980.

[28] C. P. Loizou, C. S. Pattichis, C. I. Christodoulou, R. S. H. Istepanian, M. Pantziaris, and A. Nicoliades, "Despeckle filtering in ultrasound imaging of the carotid artery," *IEEE Trans. Ultrason. Feroelectr. Freq. Control*, vol. 52, no. 2, pp. 1653–1669, 2005.

[29] C. P. Loizou, T. Kasparis, P. Christodoulides, C. Theofanous, M. Pantziaris, E. Kyriakou, and C. S. Pattichis, "Despeckle filtering in ultrasound video of the common carotid artery," in *Proc. IEEE 12th Int. Conf. Bioinformatics and Bioengineering*, 2012, pp. 721–726.

[30] C. P. Loizou, T. Kasparis, P. Papakyriakou, L. Christodoulou, M. Pantziaris, and C. S. Pattichis, "Video segmentation of the common carotid artery intima-media complex," in *Proc. IEEE 12th Int. Conf. Bioinformatics and Bioengineering*, 2012, pp. 500–505.

[31] A. Roy, S. Sural, J. Mukherjee, and A. K. Majunmdar, "State based modeling and object extraction from echocardiogram video," *IEEE Trans. Inf. Technol. Biomed.*, vol. 12, no. 3, pp. 366–376, 2008.

[32] C. P. Loizou, M. Pantziaris, C. S. Pattichis, and E. Kyriakou, "M-mode state-based identification in ultrasound videos of the common carotid artery," in *Proc. 4th Int. Symp. Communications, Control and Signal Processing*, 2010, pp. 1–6.

[33] C. Metz, "Basic principles of ROC analysis," *Semin. Nucl. Med.*, vol. 8, no. 4, pp. 283–298, 1978.

[34] S. Golemati, J. S. Stoitsis, A. Gastounioti, A. C. Dimopoulos, V. Koropouli, and K. S. Nikita, "Comparison of block matching and differential methods for motion analysis of the carotid artery wall from ultrasound images," *IEEE Trans. Inf. Technol. Biomed.*, vol. 16, no. 5, pp. 852–858, 2012.

[35] E. Brusseau, C. L. De Korte, F. Mastick, J. Schaar, and A. F. W. Van der Steen, "Fully automatic luminal contour segmentation in intracoronary ultrasound imaging—A statistical approach," *IEEE Trans. Med. Imaging*, vol. 23, no. 5, pp. 554–566, 2004.

[36] M. E. Olszewski, A. Wahle, S. C. Vigmostad, and M. Sonka, "Multidimensional segmentation of coronary intravascular ultrasound images using knowledge-based methods," in *Proc. SPIE*, 2005, vol. 5747, pp. 496–504.

[37] M.-J. Jurasic, A. Lovrencic-Huzjan, M. R. Bedekovic, and V. Demarin, "How to monitor vascular aging with an ultrasound," *J. Neurol. Sci.*, vol. 257, no. 1–2, pp. 139–142, 2007.

[38] S. Ebadollahi, S. F. Chang, and H. Wu, "Automatic view recognition in echocardiogram videos using parts-based representation," in *Proc. IEEE Computer Society Conf. Computer Vision and Pattern Recognition*, 2004, vol. 2, pp. 2–9.

[39] S. Kevin, J. H. Park, B. Georgescu, C. Simopoulos, J. Otsuki, and D. Comaniciu, "Image-based multiclass boosting and echocardiographic view classification," in *Proc. IEEE Computer Society Conf. Computer Vision and Pattern Recognition*, 2006, vol. 2, pp. 1559–1565.

[40] A. Landry, J. D. Spence, and A. Fenster, "Measurement of carotid plaque volume by 3-dimensional ultrasound," *Stroke*, vol. 35, no. 4, pp. 864–869, 2004.

[41] B. Chiu, M. Egger, J. D. Spence, G. Parraga, and A. Fenster, "Quantification of carotid vessel wall and plaque thickness change using 3D ultrasound images," *Med. Phys.*, vol. 35, no. 8, pp. 3691–3710, Aug. 2008.

[42] B. Chiu, M. Egger, J. D. Spence, G. Parraga, and A. Fenster, "Development of 3D ultrasound techniques for carotid artery disease assessment and monitoring," *Int. J. CARS*, vol. 3, no. 1–2, pp. 1–10, 2008.

[43] C. I. Christodoulou, C. S. Pattichis, M. Pantziaris, and A. Nicolaides, "Texture based classification of atherosclerotic carotid plaques," *IEEE Trans. Med. Imaging*, vol. 22, no. 7, pp. 902–912, July. 2003.

[44] E. Kyriacou, C. Pattichis, M. Pattichis, C. P. Loizou, C. Christodoulou, S. Kakos, and A. Nicolaides, "A review of non-invasive ultrasound imaging processing methods in the analysis of carotid plaque morphology for the assessment of stroke," *IEEE Trans. Inf. Technol. Biomed.*, vol. 14, no. 4, pp. 1027–1038, 2010.

[45] M. Cinthio, A. S. Ahlgren, J. Bergkvist, T. Jansson, H. W. Person, and K. Lindstrom, "Longitudinal movements and resulting shear strain of the arterial wall," *Am. J. Physiol. Heart Circ. Physiol.*, vol. 291, no. 1, pp. H394–H402, 2006.

[46] H. Nasrabadi, M. S. Pattichis, P. Fisher, A. N. Nicolaides, M. B. Griffin, G. Makris, E. C. Kyriacou, and C. S. Pattichis, "Measurement of motion of carotid bifurcation plaques," in *IEEE 12th Int. Conf. Bioinformatics and Bioengineering*, 2012, pp. 506–511.

[47] S. Osher and J. A. Sethian, "Fronts propagating with curvature-dependent speed: Algorithms based on Hamilton-Jacobi formulations," *J. Comput. Phys.*, vol. 79, no. 1, pp. 12–49, 1988.

[48] D. Mumford and J. Shah, "Optimal approximation by piecewise smooth functions and associated variational problems," *Commun. Pure Appl. Math.*, vol. 42, no. 5, pp. 577–685, 1989.

[49] E. D. Angelini, S. Homma, G. Pearson, J. W. Holmes, and A. F. Laine, "Segmentation of real-time three-dimensional ultrasound for quantification of ventricular function: A clinical study on right and left ventricles," *Ultrasound Med. Biol.*, vol. 31, no. 9, pp. 1143–1158, 2005.

Christos P. Loizou (SM'05) received the B.Sc. degree in electrical engineering and the Dipl.-Ing. (M.Sc.) degree in computer science and telecommunications from the University of Kaisserslautern, Kaisserslautern, Germany, in 1986 and 1990, respectively, and the Ph.D. degree in ultrasound image analysis of the carotid artery from the Department of Computer Science, Kingston University, London, UK, in 2005. From 1996 to 2000, he was a Lecturer in the Department of Computer Science, Higher Technical Institute, Nicosia, Cyprus. Since 2000, he has been an Assistant Professor in the Department of Computer Science, Intercollege, Cyprus. He was a supervisor of a number of Ph.D. and B.Sc. students in computer image analysis and telemedicine. He is also an Associate Researcher at the Institute of Neurology and Genetics, Nicosia, Cyprus, and at the Cyprus University of Technology, Limassol, Cyprus. He is the author or coauthor of the book *Despeckle Filtering Algorithms and Software for Ultrasound Imaging*, one more book, 12 chapters in books, 23 refereed journals, and 52 conference papers in image and video analysis. His research interests include medical imaging and processing; motion and video analysis; signal and image processing; pattern recognition; biosignal analysis in ultrasound, magnetic resonance, and optical coherence tomography imaging; and computer applications in medicine. Dr. Loizou is a Senior Member of the IEEE, and serves as a reviewer in many IEEE Transactions journals and as a chair or co-chair in many IEEE conferences.

Styliani Petroudi received her B.Sc. degree in electrical engineering in 1998 with a Fulbright Scholarship from the University of Michigan, Ann Arbor, where she also received her M.Sc. degree in electrical engineering with a focus in signals and systems in 2000. Styliani continued her Ph.D. studies with a Cancer Research U.K. fellowship at the University of Oxford, where she received the D. Phil. degree in 2005. From 2005 to 2007, she was a Postdoctoral Research Associate at the Wolfson Medical Vision Lab, Department of Engineering, Oxford University, working on oncological image analysis. Since 2007, she has been working at the University of Cyprus as a Visiting Lecturer in the Department of Electrical and Computer Engineering, and then as a Research Fellow in the Department of Computer Science. Styliani's research interests lie in the areas of signal processing, medical image analysis with applications in oncological imaging, computer-assisted minimally invasive surgery, and artificial intelligence for the advancement of detection and diagnosis schemes that improve clinical outcomes.

Marios Pantziaris received the M.D. degree in neurology from the Aristotelion University, Thessaloniki, Greece, in 1995. Currently, he is working with the Cyprus Institute of Neurology and Genetics, Nicosia, Cyprus, as a Senior Neurologist in the Neurological Department and is the Head of the Neurovascular Department. He has been trained in carotid duplex–Doppler ultrasonography at St. Mary's Hospital, London, in 1995. In 1999, he was a visiting doctor in acute stroke treatment at Massachusetts General Hospital, Harvard University, Boston. He has considerable experience in carotid–transcranial ultrasound, has participated in many research projects, and has several publications to his name. He is also the Head of the Multiple Sclerosis (MS) Clinic, where he is running research projects towards the etiology and therapy of MS.

Andrew N. Nicolaides is a graduate of the Pancyprian Gymnasium, Nicosia, and Guy's Hospital Medical School, London University (1962), and a fellow of the Royal College of Surgeons England and the Royal College of Surgeons Edinburgh (1967). His higher surgical training was at Oxford University, Kings College Hospital Medical School, London, UK, and St. Mary's Hospital Medical School, London, UK. He was awarded the Jacksonian prize by the Royal College of Surgeons England in 1972 for his work on the prevention of venous thromboembolism and obtained the degree of M.S. (Master of Surgery) in 1976. He was the Professor of Vascular Surgery at the Imperial College School of Medicine (St. Mary's Hospital) and Consultant Vascular Surgeon at St. Mary's Hospital from 1983 to 2000, and Medical Director of the Cyprus Institute of Neurology and Genetics, Nicosia, Cyprus, from 2001 to 2004. His research group is known internationally in several areas, including noninvasive vascular screening and diagnostic investigation, and early detection and prevention of cardiovascular and venous disease. His research is now directed towards the genetic risk factors for cardiovascular disease, identification of individuals at risk and the development of effective methods of prevention, especially stroke. He is Past-President of the International Union of Angiology and Past-President of the Section of Measurement in Medicine of the Royal Society of Medicine.

He has received many awards and honorary memberships from many scientific societies. He is Editor-in-Chief of *International Angiology* and is on the Editorial Board of many vascular journals. He is Professor Emeritus at Imperial College, London, UK and an examiner for M.S. and Ph.D. degrees for London University. He is a Special Scientist at the University of Cyprus, Nicosia, Cyprus, and Medical Director of the Vascular Screening and Diagnostic Centre in London. He has trained more than 200 vascular surgeons who are practicing all over the world; ten of them are holding prestigious Chairs as professors in vascular surgery. He was made Archon Megas Referendarios, an honor bestowed by the Patriarch of Constantinople in 1994. He is coauthor of more than 400 original papers and editor of 14 books.

Constantinos Pattichis (S'88–M'88–SM'99) is currently a Professor in the Department of Computer Science of the University of Cyprus. His research interests include e-health and m-health, medical imaging, biosignal analysis, life sciences informatics, and intelligent systems. He has published 78 refereed journal and 186 conference papers, and 27 chapters in books in these areas. He is co-editor of the books *M-Health: Emerging Mobile Health Systems* and *Ultrasound and Carotid Bifurcation Atherosclerosis*, published by Springer in 2006 and 2012, respectively. He was Guest Co-Editor of 11 journal Special Issues, including the more recent ones on Atherosclerotic Cardiovascular Health Informatics, and Citizen Centered e-Health Systems in a Global Healthcare Environment, of the *IEEE Transactions on Information Technology in Biomedicine.* He was General Co-Chairman of the IEEE 12th International Conference on Bioinformatics and Bioengineering (BIBE2012), and the IEEE Information Technology in Biomedicine (ITAB09). Moreover, he serves as Distinguished Lecturer of the IEEE EMBS, an Associate Editor of the *IEEE Journal of Biomedical and Health Informatics*, and is on the Editorial Board of the *Journal of Biomedical Signal Processing and Control.* He is a Fellow of IET and Senior Member of IEEE.